Aspects of Flow of Power-Law Fluids in Porous Media

C. B. Shah and Y. C. Yortsos
Dept. of Chemical Engineering, University of Southern California, Los Angeles, CA 90089

Non-Newtonian fluid flow in porous media is encountered in a variety of applications. Aspects of single-phase flow of power-law fluids in porous media are examined. First, homogenization theory is used to derive a macroscopic law. It is shown that the single-capillary power law between flow rate and pressure gradient also applies at the macroscopic scale, provided that the Reynolds number is sufficiently small. Homogenization theory confirms the validity of the use of pore network models to describe flow of power-law fluids, although not necessarily of fluids of a more general rheology. Flow in pore networks is next used to explore various pore geometry effects. Numerical simulations show that approaches based on an effective medium or on the existence of a critical path, which carries most of the flow, are valid in narrow- or wide-pore-size distributions, respectively. The corresponding expressions agreed well with the numerical results in the respective ranges. An analysis presented for Bethe lattices leads to closed-form expressions in two limits: for an effective medium and near percolation. The behavior near percolation generalizes the results of Stinchcombe (1974) for the linear (Newtonian) case.

Introduction

The flow of fluids through a variety of porous media is common to many engineering applications. In several of these, non-Newtonian fluids are extensively involved. Examples include enhanced oil recovery (EOR) processes in oil reservoirs, where low-concentration polymer solutions, emulsions, foams, gels, and so forth, are simultaneously injected with a displacing fluid (see Schurz et al., 1989). These additives divert displacing fluids by blocking flow from previously swept zones, thus leading to an improvement of sweep efficiencies. Other examples include drilling muds, typically represented as Bingham plastics (Wu et al., 1991, 1992), and heavy oils (Barenblatt et al., 1990), the rheology of which has also been approximated as a Bingham plastic.

While the flow of Newtonian fluids in porous media is well understood, the state of the art in non-Newtonian fluid flow is far from complete. This applies to both single- and multiphase flow problems, and it is due to the complexity brought about by the combination of the non-Newtonian rheology with the porous media geometry. Although many practitioners have routinely used phenomenological extensions of single-capillary flow rate–pressure drop relationships to porous media (Wu et al. 1991), a rigorous derivation of this result is still lacking. With few exceptions, laws equivalent to Darcy's for the flow of non-Newtonian fluids in porous media have not been established. The important exception concerns power-law fluids, where many experimental and theoretical studies have been undertaken.

An early review of the modeling of flow of non-Newtonian fluids in porous media was presented by Savins (1969). Most of these works developed nonlinear versions of Darcy's law by representing the porous medium as a collection of noninteracting elements (such as a collection of parallel capillaries). Bird et al. (1960) suggested a scale-up of non-Newtonian fluid flow in porous media based on capillary models. For a power-law fluid of consistency index m and power-law index n, their equation reads

$$u^n = (k_1/H)\,\frac{\Delta P}{L} \tag{1}$$

where u is the average (superficial) velocity, k_1 is the single-phase Newtonian permeability, and the parameter H is given in Table 1. Teeuw and Hesselink (1980) accounted for effects

Correspondence concerning this article should be addressed to Y. C. Yortsos.
C. B. Shah is currently with Simulation Sciences.

Table 1. Suggested Scaleup Expressions for Power-Law Fluid Flow in Porous Media

References	Parameter H
Bird et al. (1960)	$H = m\left[2\left(\frac{25}{12}\right)^n\left(\frac{3n+1}{n}\right)^n (3)^{n+1}/150\right][D_p]^{1-n}[\phi]^{2(n-1)}$
Christopher and Middleman (1965)	$H = \frac{m}{12}\left(\frac{9n+3}{n}\right)^n (150k_1\phi)^{(1-n)/2}$
Sadowski (1965)	$\frac{1}{H} = \frac{1}{\mu^0}\left[1+[4/((2n+1)/n)]\left(\frac{\tau_{RH}^{(1-n)/n}}{\tau_{1/2}}\right)\right]$, $\tau_{RH} = [\phi D_p/6(1-\phi)]\Delta P/L$
Teeuw and Hesselink (1980)	$H = 2mk_1^{(1-n)/2}\left(\frac{3n+1}{\phi n}\right)^n\left(\frac{\phi}{8}\right)^{(n+1)/2}$

of tortuosity, to obtain a modified expression for H, while Christopher and Middleman (1965) proposed a different version, based on a modification of the Blake-Kozeny equation. These results are summarized in Table 1. Analogous results were obtained for a variety of other rheologies. For example, Sadowski (1965) employed a capillary model of porous media, but used an Ellis model for the fluid. Sorbie et al. (1989) have discussed the scale-up of a Carreau fluid. Studies involving fluids, such as xanthan biopolymers, which are frequently used in displacement processes for mobility control, were undertaken by Hirasaki and Pope (1974), Willhite and Uhl (1986), and Chauveteau (1981), all with the use of power-law models. A detailed review of these works can be found in Salman (1989) and in Sorbie et al. (1989).

In more recent studies, the representation of the pore-space in terms of equivalent lattice models has reduced many porous media problems into equivalent problems of resistor networks, the conductance of which can be related to the properties of individual pore elements. In a study of Xanthan biopolymers in porous media, Cannella et al. (1988) derived a relation for its apparent viscosity in porous media based on a heuristic effective medium approximation. Sorbie et al. (1989) numerically simulated the flow of a Carreau fluid also using a network model. In an unpublished study, Sahimi and Yortsos (1990) used network models to examine various aspects of power-law fluid flow in porous media. They postulated an effective medium theory (EMT) and extended the critical path analysis (CPA) of Katz and Thompson (1986) to power-law fluids (see also Sahimi, 1993).

The use of a single capillary, and by extension of capillary networks, to model non-Newtonian flow in porous media has been questioned based on experimental findings. Sheffield and Metzner (1976) and Duda et al. (1983) conducted experiments that have suggested that the macroscale relationship between flow rate and pressure drop in a porous medium may be different from that in a single capillary. In a study of carboxymethyl cellulose and xanthan gum flow in sintered bronze disks, Duda et al. (1983) proposed that nonuniform diameter models are necessary in order to adequately characterize the macroscopic behavior. Likewise, in a study of flow of emulsions, Sheffield and Metzner (1975) found that converging-diverging pore models correlated experimental data better than the conventional capillary tube model, although they also pointed out possible limitations of such models to all porous media. Experimental studies in a sinusoidal tube, but with an emphasis on viscoelastic effects, were also carried out by Deiber and Schowalter (1981). Viscoelastic effects become significant in flow in porous media when the Deborah number exceeds a critical value. In such cases, the simple power-law capillary model is likely to fail. Some experimental studies (James and Mclaren, 1975; Durst et al., 1987; Jones and Walters, 1989) discussed the effect of the behavior of non-Newtonian fluids (mainly polymer solutions) in extension-dominated flows. Jones and Walters (1989) reported that above a critical set of conditions a significant increase in the flow resistance was observed in typical porous media geometries. They found that extensional-viscosity effects in polyacrylamide solutions were important beyond the critical strain rate region, although the effect was very weak in aqueous solutions of Xanthan gum, the behavior of which could be predicted on the basis of shear viscosity alone. In our analysis, we have neglected such issues of extensional viscosity.

Numerical studies in the flow of strictly power-law fluids in model porous media were recently conducted. In a study of the flow of a shear-thinning aqueous polyacrylamide solution through sinusoidal capillaries, Huzarewicz et al. (1991) reported that the product fRe, between the friction factor f and the Reynolds number Re, remains constant at low Re. In a different study of the flow of power-law fluids in a periodically constricted tube, Pilitsis et al. (1989) also showed that fRe is constant at small Re. These results suggest that for strictly power-law fluids and at low Re, the functional form of the single-capillary power law should be valid, regardless of the geometry of the system. Of course, this would not necessarily apply to all rheologies, and certainly not to those used in the experiments reported in Sheffield and Metzner (1976) and Duda et al. (1983). It should be pointed out that "strictly power-law fluids" are certainly quite rare (in the sense that a low-shear-rate Newtonian region instead of a power-law behavior is likely to exist).

The possibility that a macroscopic power law may exist for strictly power law fluids was suspected for some time (Table 1, for example). More recently, macroscopic power laws have been postulated for power-law resistor networks (Straley and Kenkel, 1984; Blumenfield and Aharony, 1985). Larson (1981) used a scaling argument to also propose a general macroscopic power law for the flow of power-law fluids in porous media. With the exception of a rather formal study by Bourgeat and Mikelic (1992), however, a rigorous analysis of the flow of power-law fluids in porous media is lacking. It is

the purpose of this article to address this and some related issues. Specifically, this article has the following objectives: first, to explore the averaging of flow of power-law fluids in porous media and to show that the functional form of the single-capillary model is retained, thus leading to an extension of Darcy's law. For this task, the method of homogenization for periodic structures will be used. The fluids considered are inelastic and of a power-law behavior. Having established its validity, the relevant macroscopic coefficients (permeability) will be explored in network-like porous media. In particular, the EMT and CPA approximations of Sahimi and Yortsos (1990) will be discussed. Based on the numerical solution of the corresponding network problem, these approximations will be tested. Finally, for the sake of completeness, some analytical results for Bethe lattices will also be presented.

Homogenization

To establish the validity of a macroscopic power law we shall make use of homogenization theory (see Bensoussan et al., 1978). While extensively used in Newtonian flow (see Auriault, 1980; Mei and Auriault, 1991), only a recent, but rather formal, attempt has been made for non-Newtonian fluids (Bourgeat and Mikelic, 1992). Homogenization is a powerful method, as it provides a constructive approach for the evaluation of the macroscopic transport coefficients. The theory is based on two assumptions: (1) The existence of two separated length scales, a microscale l (such as a typical pore size) and a macroscale L, the ratio of which is small, $\epsilon \equiv l/L \ll 1$; and (2) the periodicity or stationarity of the porous medium at the macroscale. Auriault (1991) has recently presented a review of standard homogenization methods.

In the present context, we consider power-law fluid flow in a periodic medium with a microstructure specified in the unit cell Ω (Figure 1). For an incompressible, inelastic fluid, the local description is given by the standard equations

$$\rho \boldsymbol{v}\cdot\nabla\boldsymbol{v} = \nabla\cdot(\eta\nabla\boldsymbol{v}) - \nabla p \tag{2}$$

$$\nabla\cdot\boldsymbol{v} = 0, \tag{3}$$

which are subject to no-slip condition at the walls of the solid matrix

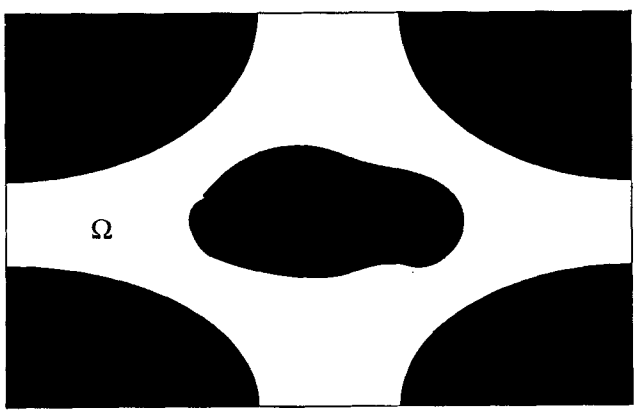

Figure 1. Schematic of unit cell.

$$\boldsymbol{v} = 0 \tag{4}$$

and to periodicity at the cell boundary $\partial\Omega$. The power-law fluid viscosity is given by (Bird et al., 1960)

$$\eta = m\left|\sqrt{\frac{1}{2}(\boldsymbol{\Delta}:\boldsymbol{\Delta})}\right|^{n-1} \tag{5}$$

where $\boldsymbol{\Delta} \equiv \frac{1}{2}(\nabla\boldsymbol{v} + \nabla\boldsymbol{v}^T)$ is the rate of deformation tensor. To proceed, dimensionless notation is introduced, by scaling viscosity by $ml^{(1-n)}v^{*(n-1)}$, velocities by a characteristic macroscale velocity v^*, and pressure by the macroscale pressure drop $\Delta p^* = ml^{-(n+1)}v^{*n}L$. By denoting the scale variables by subscript a we obtain

$$Re\boldsymbol{v}_a\cdot\nabla\boldsymbol{v}_a = \nabla\cdot(\eta_a\nabla\boldsymbol{v}_a) - \frac{1}{\epsilon}\nabla p_a \tag{6}$$

$$\eta_a = \left|\sqrt{\frac{1}{2}(\boldsymbol{\Delta}_a:\boldsymbol{\Delta}_a)}\right|^{n-1} \tag{7}$$

where the Reynolds number, $Re \equiv (\rho l^n v^{*(2-n)})/m$, was defined. For low Re values (low velocity for $n < 2$), inertia effects are negligible, leading to

$$0 = \nabla\cdot(\eta_a\nabla\boldsymbol{v}_a) - \frac{1}{\epsilon}\nabla p_a \tag{8}$$

$$\nabla\cdot\boldsymbol{v}_a = 0. \tag{9}$$

Clearly, shear-thickening fluids with $2 < n$ do not satisfy creeping-flow conditions at small velocities (see also below). To proceed with homogenization, a large (dimensionless) macroscale coordinate $\boldsymbol{X}$ is next defined,

$$\boldsymbol{X} = \epsilon\boldsymbol{x} \tag{10}$$

and the usual expansion in velocity and pressure is taken

$$\boldsymbol{v}_a = \boldsymbol{v}_a^{(0)}(\boldsymbol{x}, \boldsymbol{X}) + \epsilon\boldsymbol{v}_a^{(1)}(\boldsymbol{x}, \boldsymbol{X}) + \cdots \tag{11}$$

$$p_a = p_a^{(0)}(\boldsymbol{x}, \boldsymbol{X}) + \epsilon p_a^{(1)}(\boldsymbol{x}, \boldsymbol{X}) + \cdots, \tag{12}$$

from which it also follows that

$$\eta_a = \eta_a^{(0)}(\boldsymbol{x}, \boldsymbol{X}) + \epsilon\eta_a^{(1)}(\boldsymbol{x}, \boldsymbol{X}) + \cdots. \tag{13}$$

Next, we introduce two-timing and transform spatial derivatives according to $\nabla \to \nabla + \epsilon\nabla_X$, where we denoted gradients at the macroscale by ∇_X. Substitution and further expansion yields the set of equations

$$\nabla p_a^{(0)} = 0 \tag{14}$$

$$\nabla\cdot\boldsymbol{v}_a^{(0)} = 0 \tag{15}$$

$$\nabla\cdot\boldsymbol{v}_a^{(1)} = -\nabla_X\cdot\boldsymbol{v}_a^{(0)} \tag{16}$$

$$\nabla\cdot(\eta_a^{(0)}\nabla\boldsymbol{v}_a^{(0)}) - \nabla p_a^{(1)} = \nabla_X p_a^{(0)}, \tag{17}$$

the solution of which will be sought along with no-slip and periodicity conditions.

The solution of Eq. 14 is $p_a^{(0)} \equiv p_a^{(0)}(\boldsymbol{X})$, showing that the pressure field at zeroth order is only a function of the macroscale variable $\boldsymbol{X}$. Periodicity, no-slip, and application of Green's theorem to Eq. 16 yield the macroscale continuity equation

$$\nabla_X \cdot \langle \boldsymbol{v}_a^{(0)} \rangle = 0 \tag{18}$$

where the volume average over the cell volume $\boldsymbol{\Omega}$ was defined, $\langle \psi \rangle \equiv 1/|\Omega| \int \psi \, d\Omega$. For the derivation of the macroscale momentum equation, the solution of Eqs. 15 and 17 is necessary. The solution $\boldsymbol{v}_a^{(0)}$ may depend on the macroscale gradient $\nabla_X p_a^{(0)}$ in a generally complex fashion. However, we expect that $\boldsymbol{v}_a^{(0)}$ would vanish with $\nabla_X p_a^{(0)}$. This intuitive result can also be rigorously proved, although this will not be attempted here. Thus, we expect, without loss in generality, the relation

$$\boldsymbol{v}_a^{(0)} = -\boldsymbol{k}_a \cdot \nabla_X p_a^{(0)} \tag{19}$$

where the nonsingular tensor $\boldsymbol{k}_a$ depends on the local coordinate $\boldsymbol{x}$, and possibly on $\nabla_X p_a^{(0)}$ as well. To proceed further, we rescale once more, by scaling velocity by $N_a^{1/n}$ and pressure by N_a, where we have denoted $N_a = |\nabla_X \langle p_a^{(0)} \rangle|$, and we denote the new variables by subscript b. If $\boldsymbol{e}$ denotes the unit vector in the direction of the pressure gradient

$$\nabla_X p_b^{(0)} = -\boldsymbol{e} |\nabla_X \langle p_a^{(0)} \rangle|, \tag{20}$$

we obtain in the new notation the set of equations

$$\nabla \cdot (\eta_b^{(0)} \nabla \boldsymbol{v}_b^{(0)}) - \nabla p_b^{(1)} = -\boldsymbol{e} \tag{21}$$

$$\nabla \cdot \boldsymbol{v}_b^{(0)} = 0. \tag{22}$$

Although nonlinear, Eqs. 21 and 22 subject to no-slip and periodicity conditions can, in principle, be solved. This dimensionless solution, $\boldsymbol{v}_b^{(0)}$, may depend on the orientation of the macroscopic pressure gradient, but it is *independent* of its magnitude. By comparing with Eq. 19 we can take

$$\boldsymbol{v}_b^{(0)} = \boldsymbol{k}_b \cdot \boldsymbol{e} \tag{23}$$

where dimensionless tensor $\boldsymbol{k}_b$ is also independent of the pressure gradient. A volume averaging of this equation then gives

$$\langle \boldsymbol{v}_b^{(0)} \rangle = -\boldsymbol{K} \cdot \frac{\nabla_X \langle p_b^{(0)} \rangle}{|\nabla_X \langle p_b^{(0)} \rangle|} \tag{24}$$

where the dimensionless tensor $\boldsymbol{K} = \langle k_b \rangle$ is independent of the macroscale pressure gradient, and it is to be determined from the microstructure. In principle, the computation of $\boldsymbol{K}$ is possible. Having determined the functional relationship (Eq. 24), we proceed to scale back to the original variables, remove superscript (0) and the averaging symbol, and obtain after some calculations the following dimensional result

$$\boldsymbol{v} = -\left(\frac{l^{(1+n)/n}}{m^{1/n}} \right) |\nabla p|^{(1/n)-1} \boldsymbol{K} \cdot \nabla p \tag{25}$$

where we reverted to the usual notation for the gradient. This is the final macroscopic law relating the flow of power-law fluids in the limit of small *Re*. It becomes evident that the single-capillary power-law relationship has survived the averaging process, as is also suggested in the simpler models of sinusoidal capillaries.

Equation 25 represents a rigorous extension of Darcy's law to power-law fluid flow in porous media. As just mentioned, tensor $\boldsymbol{K}$ may depend in general on the orientation of the pressure gradient. In particular, when applied to one-dimensional (1-D) flows, Eq. 25 can be equivalently expressed by Eq. 1, where parameter H is now identified as

$$H = \frac{km}{K_{11}^n l^{1+n}}. \tag{26}$$

In the next sections, we use simple network models to obtain an insight on the dependence of this coefficient on simple geometrical properties of the porous medium.

Network Models for Flow of Power-Law Fluids

Having established the validity of a power-law description, we proceed next with a simplified solution of the flow problem for porous media that can be represented as networks of capillaries. This approach was also used by Sorbie et al. (1989) in their study of non-Newtonian flow, although it has its origin in much earlier investigations (Fatt, 1956; Simon and Kelsey, 1971; Koplik, 1982). In the simulations we used square lattices for 2-D and cubic lattices for 3-D geometries. Analytical results for Bethe lattices were also derived, and they are presented in another section. Two basic assumptions are made: (1) The fluid is homogeneous, such that adsorption, excluded volume, and so forth (Sorbie, 1989) are not considered. These effects are of course important in some practical applications. (2) Pressure drops are associated only with the bonds of the network, with the volumetric flow rate q_i through bond i related to the pressure drop Δp_i by the power law

$$q_i = g_i (\Delta p_i)^{1/n} \tag{27}$$

where g_i is the bond conductance. Steady-state flow in a single capillary of (distributed) radius r_i and (constant) length l gives

$$g_i = \frac{\pi n r_i^{(3n+1)/n}}{(3n+1)(2lm)^{1/n}}. \tag{28}$$

The sensitive dependence of the conductance g on the capillary radius r for small n should be noted. The flow problem was solved by formulating mass balances at each node of the network (Koplik, 1982, and Sorbie et al., 1989) and solving the resulting set of nonlinear algebraic equations using a successive overrelaxation (SOR) method. Simulations were done in 2-D and 3-D lattices of various sizes (typically 100×100 in 2-D and $11 \times 11 \times 11$ in 3-D) and pore-size distributions. For purposes of testing the CPA predictions, we used uniform

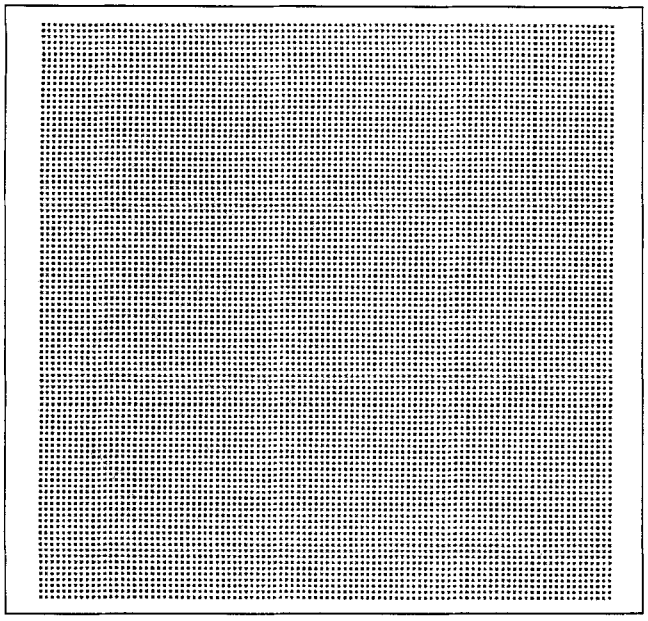

Figure 2. Flow pattern for $n = 0.2$ in [0.9–1.1].

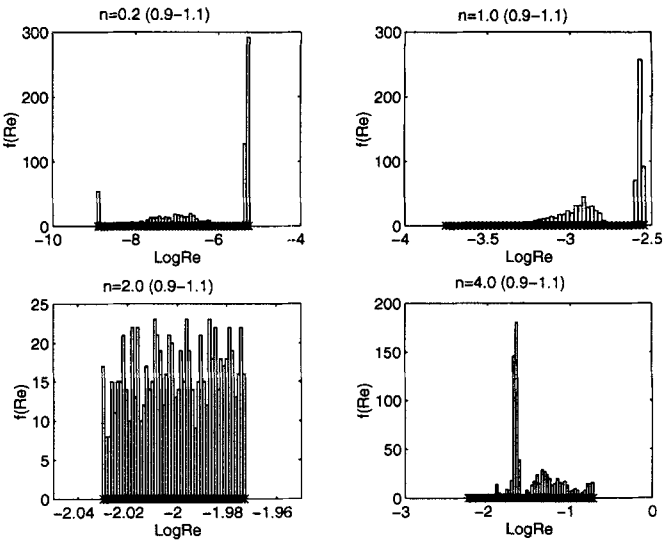

Figure 3. Local Reynolds number distribution for different n in [0.9–1.1].

pore-size distributions that varied from narrow [0.9–1.1] to wide [0.01–1.99] in normalized notation.

Steady-state flow patterns for various conditions are shown in Figures 2, 4, and 5. In these figures, the intensity of the flow rate through each bond is proportional to the level of grayness, with black representing maximum flow rate. Only flow through the bonds is shown, flow through the connecting nodes being depicted in white. Figure 2 shows the flow pattern for $n = 0.2$ in a 100×100 square lattice consisting of the narrow pore-size distribution [0.9–1.1]. As expected for such distributions, the flow is evenly distributed through the bonds aligned with the pressure gradient and it is negligible on the bonds perpendicular to it. Identical patterns were obtained for all other values of n tested. *Effective medium* theories are expected to be quite applicable for such narrow pore-size distributions. The corresponding distribution of the local Reynolds numbers (Figure 3) shows that in such narrow-size distribution, the velocity distribution is sharply peaked. The exception is the case $n = 2$, where the Re is independent of velocity, as pointed out earlier. Incidentally, we note that the levels of Re decreases in Figure 3 do not actu-

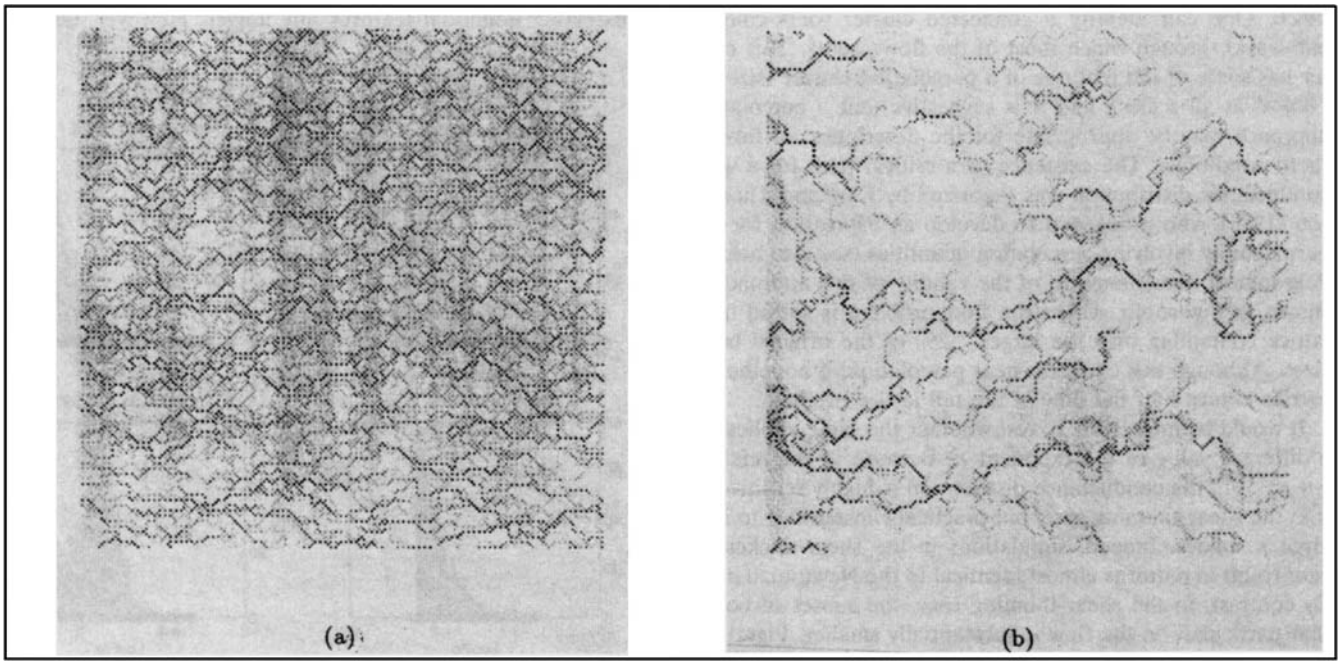

Figure 4. Flow pattern for $n = 1$ in [0.01–1.99].

(a) All bonds participating; (b) 52% of bonds participating.

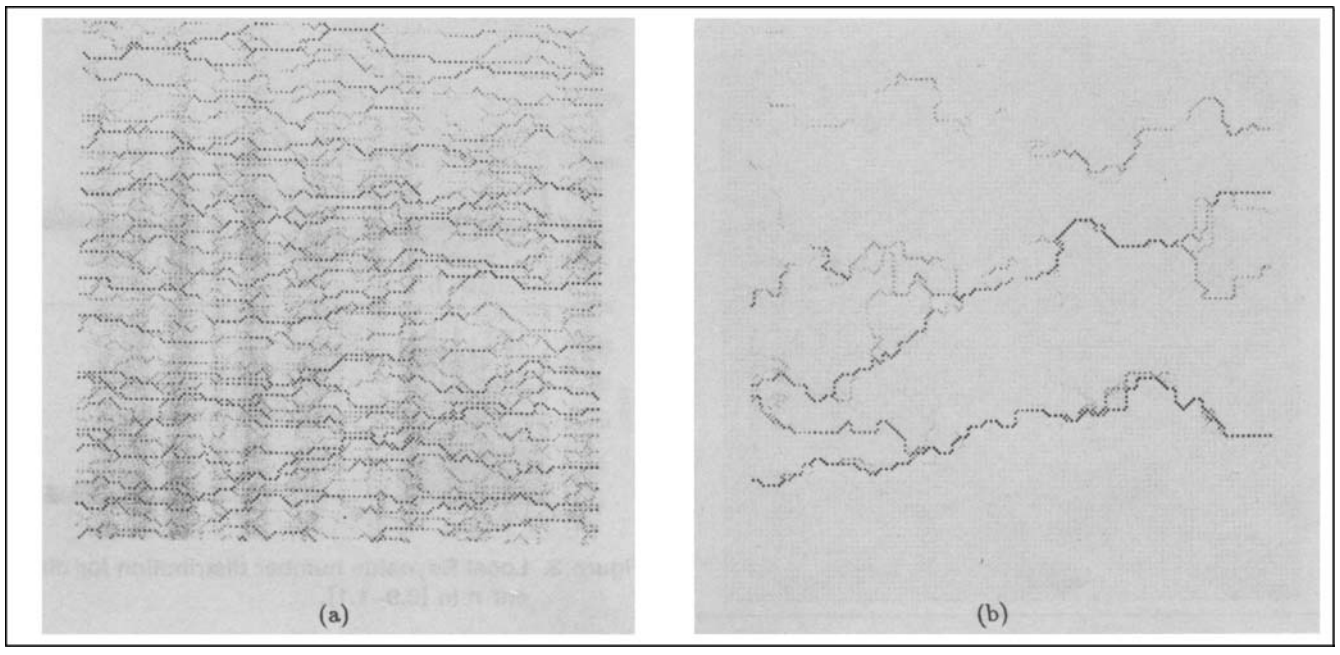

Figure 5. Flow pattern for $n = 0.2$ in [0.01–1.99].

(a) All bonds participating; (b) 52% of bonds participating.

ally reflect a physical tendency, but arise due to the particular scheme used. However, the width of the *Re* distribution does increase as n decreases.

Figure 4a shows a flow pattern for the Newtonian case ($n = 1$) for the wide pore-size distribution [0.01–1.99]. It is apparent that now the flow pattern deviates substantially from the uniform pattern of Figure 2. There exist many regions (empty pockets) in the network, where the flow rates are very small, and which contribute little to the overall flow conductance. One can identify a connected cluster (dark-colored pathways) through which most of the flow occurs. This cluster has some of the features of a percolation cluster (sizes of "holes" at all scales), and it is suggestive that a percolation approach may be appropriate for the description of flow at these conditions. The existence of a critical path for a wide conductance distribution was theorized by Katz and Thompson (1986), who proceeded to develop an expression for the permeability involving percolation quantities (see also below). A graphical demonstration of the validity of this approach is shown in Figure 4b, where the flow problem is solved on a lattice containing only the largest 52% of the original bond sizes. Although this cluster is near percolation, it nonetheless carries almost half the flow of the full lattice problem.

It would be interesting to test whether the same applies for a different value of the exponent n. Because of the relation $g \sim r^{3+(1/n)}$, the conductance distribution is highly sensitive to n in the shear-thinning case, but practically insensitive to it at large n values. Indeed, simulations in the shear-thickening case result in patterns almost identical to the Newtonian case. By contrast, in the shear-thinning case, the subset of bonds that participate in the flow is substantially smaller. Figure 5a shows a typical example for $n = 0.2$. Here, flow occurs over a sparser network of connecting bonds with most of the flow occurring over a few connected paths only. Figure 5b shows the corresponding flow pattern for a lattice containing only the largest 52% of the bonds, as is also done in Figure 4b. Although this cluster is quite sparse, the amount of flow it carries is a substantial fraction of the flow in the full problem. An even smaller participation of the total lattice in the flow exists in the small n limit, which approaches the flow behavior of a Bingham plastic (Shah et al., 1995). The corresponding *Re* distributions are shown in Figure 6. We note that the distributions are much wider than in Figure 3, not possessing unimodal features any longer. However, because

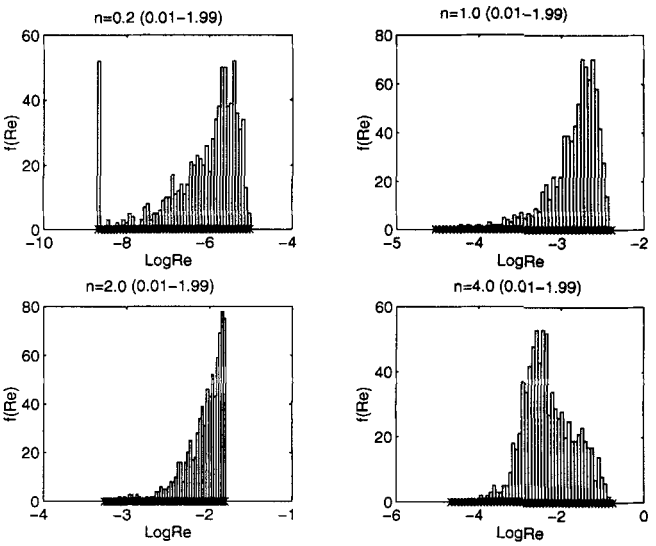

Figure 6. Local Reynolds number distribution for different n in [0.01–1.99].

of the logarithmic scale in the distributions, it is apparent that only a small subset of the network makes a significant participation to the total flow. We shall explore below whether these patterns actually reflect a critical path for power-law flow.

To analyze quantitatively flow in porous media, several theoretical tools exist. They include EMT, CPA, renormalization methods, and percolation. Many of these have been successfully applied to Newtonian flow. Recently, some EMT and CPA techniques were also developed for power-law resistors (Cannella et al., 1988; Sahimi and Yortsos, 1990; Sahimi, 1993). We use the numerical scheme to test their predictions.

Effective medium theory

EMT has often been applied to obtain estimates for the permeability of Newtonian flow in porous media (Koplik, 1981). The theory was originally developed to estimate the effective electrical conductivity of a network of linear resistors with randomly distributed conductances. For a network of resistors with conductance distribution $G(g)$, the effective conductance of a resistor of the effective medium, g_m, is the solution of

$$\int_0^\infty \frac{(g_m - g)}{[g + (Z/2 - 1)g_m]} G(g)\, dg = 0 \qquad (29)$$

where Z is the coordination number of the network. Recently, Cannella et al. (1988) advanced some heuristic arguments to extend EMT to flow of power-law fluids. They proposed that g_m can be obtained from the solution of the equation

$$\int_0^\infty \left[\left(\frac{Zg_m/2}{g + (Z/2 - 1)g_m} \right)^n - 1 \right] G(g)\, dg = 0. \qquad (30)$$

Yet another expression, which is also the asymptotic solution at large Z, can be derived for a Bethe lattice (Sahimi and Yortsos, 1990). The final equation reads

$$\int_0^\infty \left[\frac{(Z-1)g}{\{g^n + [(Z-1)^n - 1]g_m^n\}^{1/n}} - 1 \right] G(g)\, dg = 0, \quad (31)$$

which is clearly different from Eq. 30. The details of this derivation are described below in the section discussing Bethe lattices.

To test the validity of the two EMT equations, Eqs. 30 and 31, we compared their predictions with the numerical simulations for different values of the power-law index n and for different pore-size distributions. We used narrow [0.9–1.1], medium [0.4–1.6], and wide [0.01–1.99] distributions, all normalized with a mean pore size. All simulations were done in 3-D lattices. The values $Z = 6$ and $Z = 5$ (so that cubic and Bethe lattices have the same percolation threshold) were used to test the two equations, respectively. Figure 7 shows plots of the effective medium conductance g_m vs. the power-law index n. For the narrow pore-size distribution (Figure 7a), the values of g_m calculated from the analytical expressions are in good agreement with the numerical results for a wide

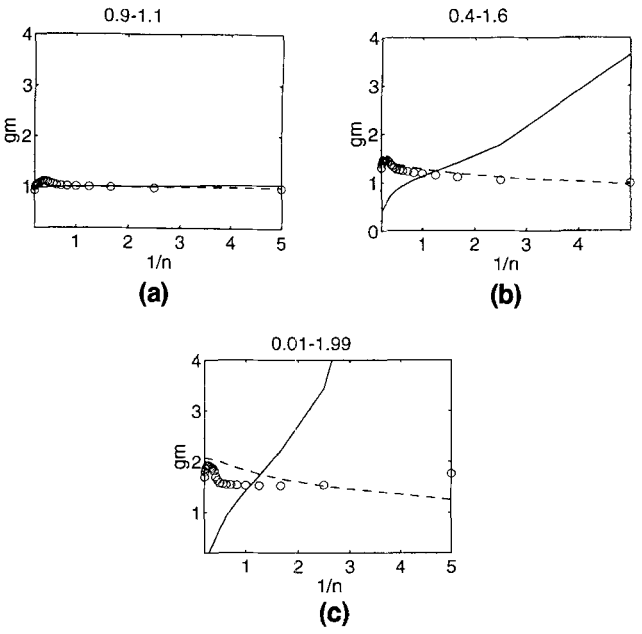

Figure 7. Effective medium conductance g_m for a pore-size distribution in (a) [0.9–1.1]; (b) [0.4–1.6]; and (c) [0.01–1.99].

○, Numerical result; –, Cannella et al. (1988); – – –, Sahimi and Yortsos (1990).

range of n, covering both shear-thinning and shear-thickening fluids. To a certain degree, this could be anticipated from the condition for the validity of the EMT and from the associated flow patterns (Figures 2 and 3). Expression 31 seems to fit the numerical value more closely, however, and also has the proper trend over the entire range of n, in contrast to Eq. 30, which for $n > 1$ has the opposite trend. Figure 7b shows the comparison for intermediate pore-size distributions. Here, expression 30 finds much less agreement with the numerical results, while it also maintains the reverse trend in the shear-thickening case. By contrast, expression 31 gives values quite close to the numerical results. However, the agreement worsens as the pore-size distribution becomes wider (Figure 7c), as expected. One concludes that under conditions, where one expects the EMT to be valid, expression 31 derived from Bethe lattices for power-law flow, is reasonably accurate for a wide range of n, covering both shear-thinning and shear-thickening fluids. Additional implications of these results are presented in the section on Bethe lattices.

Critical path analysis

In an important paper, Katz and Thompson (1986) proposed that for a porous medium with a wide pore-size distribution, flow mostly occurs over a connected cluster, the geometry of which resembles a percolation cluster. This approach actually originated from Ambegaokar et al. (1971), who studied electron transport in amorphous semiconductors. According to the argument, transport in a random system with a broad distribution of conductances is dominated by those conductances with magnitude greater than a critical

value, g_c, such that these conductances first form a sample-spanning connected cluster. Figure 4 of the numerical simulation appears to provide qualitative support for this argument for the linear case ($n=1$). Using well-known scaling laws for the conductance of a percolating cluster, Katz and Thompson (1987) subsequently proposed a model that relates the single-phase Newtonian permeability of a porous medium, k_1, to the formation factor, F, and to the characteristic length, l_c, that denotes the onset of capillary invasion in the porous medium,

$$k_1 = \frac{l_c^2}{226F}. \tag{32}$$

A similar methodology can also be applied to a network of power-law elements. This approach was for the first time introduced in Sahimi and Yortsos (1990), its details being summarized in Sahimi (1993). The calculations are straightforward, except that now one needs to use scaling laws for the power-law conductance near percolation (Straley and Kenkel, 1984; Blumenfeld and Aharony, 1985; Blumenfeld et al., 1986). The final result reads

$$q^n = \frac{k_1 A k_1^{(n-1)/2} \Delta P}{mL} \tag{33}$$

where the constant A is related to F, n, and the medium porosity ϕ by

$$A = \left[\left(\frac{1}{F}\right)^{0.436} \phi^{0.0638}\right]^{n-1} \times \left[\frac{(10.62)^{1-n} 3^{1+n} (23.51 t_n)^{nt_n}}{2^{n+2}((1+3n)/n)^n (3+t_n)^{1.12+2.76n}}\right]. \tag{34}$$

Exponent t_n scales the conductance of a percolating network of power-law resistors. For example, for a 3-D network we have (Straley and Kenkel, 1982)

$$t_n \approx 1.76 + 0.12/n. \tag{35}$$

We must point out that expression 34 differs slightly from that presented in Sahimi and Yortsos (1990) due to a calculation error.

The existence of a critical path requires a broad conductance distribution, such that substantial flow occurs only over a subset of the pore network, which can be taken to be close to the percolation cluster. Figures 4 and 5 suggest that such a critical path may in fact develop in these flows. To quantitatively test the theoretical results (Eqs. 33–35), we simulated flow of power-law fluids in a 3-D ($11\times11\times11$) lattice, with the power-law index n varied in the range [0.2, 2]. To test theory and simulation, we rearranged expressions 33 to 35 to read

$$\log(q^n/D) = \frac{1}{2}[\log k_1 + \log C^2]n + \log B \tag{36}$$

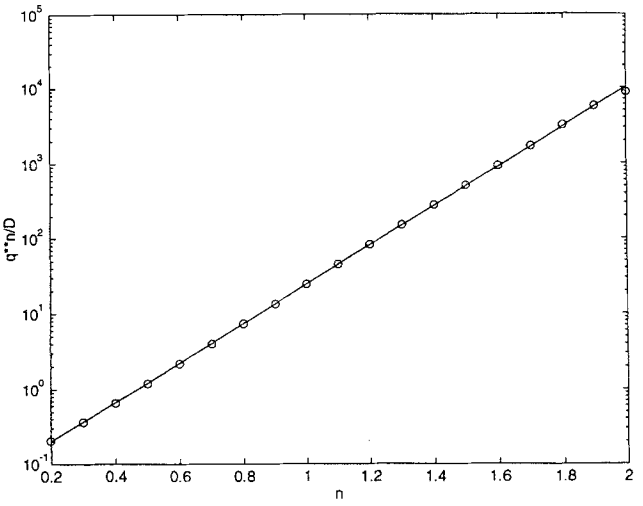

Figure 8. Test of CPA for the distribution in [0.01–1.99].

where we defined the auxiliary constants

$$D = \frac{(10.62)^{1-n} 3^{1+n} (27.51 t_n)^{nt_n}}{2^{n+2}(3n+1/n)^n (3+t_n)^{1.12+2.76n}} \tag{37}$$

$$C = \left(\frac{1}{F}\right)^{0.436} \phi^{0.0638} \tag{38}$$

and

$$B = \frac{k_1^{1/2} \Delta P}{cmL}. \tag{39}$$

In this form, we can directly test the theory by searching for a linear relation between q^n/D and n in a semilog plot. Figure 8 shows this plot for a wide distribution of pore sizes. It is apparent that the theoretical prediction (Eq. 36) of a straight line is well satisfied for all values of n. Various other size distributions also showed a similar agreement. This can be justified because of the conductance scaling $g \sim r^{(3+1)/n}$, which for small n is sufficiently sensitive to satisfy the CPA conditions for a variety of size distributions.

The preceding simulations confirmed the qualitative accuracy of EMT and CPA approximations under various conditions. We must note, however, that either theory is expected to lose accuracy when n tends to zero (where the fluid behaves similarly to a Bingham plastic). Flow of a Bingham plastic in a porous medium is discussed in a different publication (Shah et al., 1995).

Bethe Lattices

We complete this article by presenting some analytical results for a Bethe lattice. As is well known, a Bethe lattice lacks reconnections (Figure 9). This rather unrealistic feature can be useful in the derivation of closed-form expressions. We consider a Bethe lattice, across each bond of which the power law

$$q_i^n = \sigma_i \Delta p_i \tag{40}$$

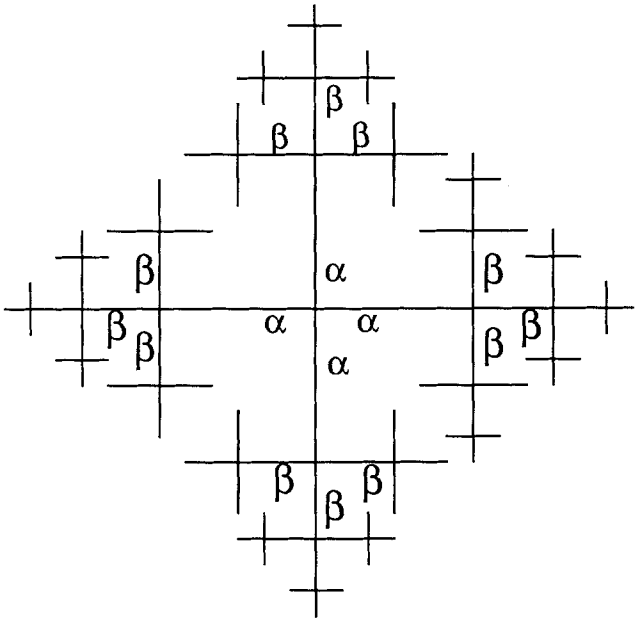

Figure 9. Bethe lattice with $Z = 4$.

is assumed to hold. Variable σ is distributed with a distribution $S(\sigma)$. Following Stinchcombe (1974), we consider the overall value $\sigma\{\alpha\}$ of a branch of bonds α (Figure 9). From the additivity rules in series and in parallel, we have

$$\sigma^{1/n}\{\alpha\} = \sum_{\beta=1}^{Z-1} \sigma_\beta^{1/n} = \sum_{\beta=1}^{Z-1} \left[\frac{1}{\sigma\{\beta\}} + \frac{1}{\sigma_\beta} \right]^{-1/n} \tag{41}$$

where $\sigma\{\beta\}$ denotes the value of branch β, all $Z-1$ of which are "daughters" of branch α. Since σ is distributed, $\sigma\{\beta\}$ is also distributed. Equivalently, we can define the conductance $\upsilon \equiv \sigma^{1/n}$, the distribution p_υ of which is obtained from $S(\sigma)$ following $p_\upsilon(\upsilon)\, d\upsilon = S(\sigma)\, d\sigma$, and the additional variables $V_\alpha \equiv \sigma^{1/n}\{\alpha\}, \ldots$. In this notation, Eq. 40 reads $q_i = \upsilon_i \Delta p_i^{1/n}$. This is equivalent to expression 27 in the previous section, although, for notational convenience, we have denoted here the conductance by υ. Then, we have

$$V_\alpha = \sum_{\beta=1}^{Z-1} \left[\frac{1}{\upsilon_\beta^n} + \frac{1}{V_\beta^n} \right]^{-1/n}. \tag{42}$$

To find the distribution of V, we can write the general equation (Heinrichs and Kumar, 1974)

$$p_V(V) = \int \cdots \int \delta\left(V - \sum_{i=1}^{Z-1} \left[\frac{1}{\upsilon_i^n} + \frac{1}{V_i^n} \right]^{-1/n} \right) \times \prod_{1}^{Z-1} p_\upsilon(\upsilon_i) p_V(V_i)\, d\upsilon_i\, dV_i. \tag{43}$$

The solution of this integral equation is sought using a Laplace transform

$$P_V(s) = \int_0^\infty p_V(V) e^{-sV}\, dV, \tag{44}$$

from which we can rewrite

$$P_V(s) = \int \cdots \int \exp\left(-s \sum_{i=1}^{Z-1} \left[\frac{1}{\upsilon_i^n} + \frac{1}{V_i^n} \right]^{-1/n} \right) \times \prod_{1}^{Z-1} p_\upsilon(\upsilon_i) p_V(V_i)\, d\upsilon_i\, dV_i$$

$$= \left[\int_0^\infty \int_0^\infty \exp\left[-s \left(\frac{1}{\upsilon^n} + \frac{1}{V^n} \right)^{-1/n} \right] \times p_\upsilon(\upsilon) p_V(V)\, d\upsilon\, dV \right]^{Z-1}. \tag{45}$$

In the notation of Stinchcombe (1974), Eq. 45 can also be expressed as $P_V(x) = [C(x)]^{Z-1}$, where

$$C(x) \equiv \int_0^\infty \int_0^\infty \exp\left[-x \left(\frac{1}{\upsilon^n} + \frac{1}{V^n} \right)^{-1/n} \right] p_\upsilon(\upsilon) p_V(V)\, d\upsilon\, dV.$$

In the Newtonian limit, Eq. 45 becomes identical to the equation derived by Heinrichs and Kumar (1974). The solution of this equation will be sought in two special limits, one for an effective medium and another for a percolating system.

Effective medium

In an effective medium, the probability distribution $p_V(V)$ is expected to peak around a mean value V^*. Heuristically, therefore, we can approximate it by a delta function (see also below). Then, $P_V(s) \simeq \exp(-sV^*)$, and we further get

$$P_V(s) \simeq \exp(-sV^*) \simeq \left[\int_0^\infty \exp\left[-s \left(\frac{1}{\upsilon^n} + \frac{1}{(V^*)^n} \right)^{-1/n} \right] p_\upsilon(\upsilon)\, d\upsilon \right]^{Z-1}. \tag{46}$$

To obtain an equation for V^* we take the derivative of Eq. 46 with respect to s and evaluate at $s = 0$ to find

$$\int_0^\infty \left[\left(\frac{1}{\upsilon^n} + \frac{1}{(V^*)^n} \right)^{-1/n} - \frac{V^*}{Z-1} \right] p_\upsilon(\upsilon)\, d\upsilon = 0. \tag{47}$$

The solution of this integral equation gives V^*. In turn, the effective bond conductance, υ_m, follows from solving Eq. 47 by assuming a delta function for both p_υ and p_V; hence

$$(V^*)^n = \upsilon_m^n [(Z-1)^n - 1]. \tag{48}$$

When combined with Eq. 47, this gives the final equation for υ_m

$$\int_0^\infty \left[\frac{(Z-1)\upsilon}{\{\upsilon^n + [(Z-1)^n - 1]\upsilon_m^n\}^{1/n}} - 1 \right] p_\upsilon(\upsilon)\, d\upsilon = 0. \tag{49}$$

In terms of the conductances of the previous sections, Eq. 49 can also be expressed as

$$\int_0^\infty \left[\frac{(Z-1)g}{\{g^n + [(Z-1)^n - 1]g_m^n\}^{1/n}} - 1 \right] G(g)\, dg = 0. \quad (50)$$

This equation generalizes the corresponding EMT equation for the case $n = 1$. It should be pointed out that the same equation also results rigorously as the leading order approximation for small s. The approach is to take an expansion in terms of generalized delta functions, $p_V = \sum_0^\infty b_m \delta^{(m)}(V - V^*)$ and to write $C(s) = \exp(sC'(0))(1 + \sum_2^\infty a_m s^{(m)})$, where a_m and b_m are coefficients to be determined by matching powers of s. Substitution in Eq. 45 leads to a series of equations. The first nontrivial result contains terms that involve Z and, in the limit of large Z, yields the preceding equation. The analysis of Eq. 50 was extensively discussed in the previous section.

It is of interest to consider some special limits of Eq. 49: For parallel capillaries ($Z \gg 1$), the solution is the arithmetic average, while for a chain ($Z = 2$), it is the harmonic average $[\int_0^\infty p_v(v) v^{-n}\, dv]^{-1/n}$. In the limit of small n the problem should approach flow with a yield stress (similar to Bingham plastic flow). We rearrange by introducing a resistance $r \equiv v^{-n}$ and its probability density function $R(r)$. Substituting in Eq. 49 and taking the limit $n \ll 1$ leads to the following

$$\int_0^\infty R(r) \exp\left(-\frac{r}{x^*} \right) dr = p_c \quad (51)$$

where we have also introduced the new variable $x^* = r^* n$. Since Eq. 51 yields a finite solution for x^*, the effective resistance, r^*, should become infinitely large in the limit of small n. Following a similar analysis for the other limit (large n), one obtains the explicit result

$$r^* = \frac{\exp\left(\int_0^\infty R(r) \ln r\, dr \right)}{(Z-1)^n}, \quad (52)$$

which shows that in this limit the effective resistance vanishes, with the large r bonds contributing the majority of the resistance.

Percolation

We consider, next, the behavior near the percolation threshold, where a fraction p of bonds is conducting. We take

$$p_v(v) = (1-p)\delta(v) + p h(v) \quad (53)$$

where $\int_0^\infty h(v)\, dv = 1$ and $\delta(x)$ denotes the delta function. Substitution in Eq. 45 gives the integral equation

$$P_V(s) = \left[1 - p + p \int_0^\infty h(v) \int_0^\infty \times \exp\left[-s \left(\frac{1}{v^n} + \frac{1}{V^n} \right)^{-1/n} \right] p_V(V)\, dv\, dV \right]^{Z-1}. \quad (54)$$

Near the percolation limit, $p = p_c(1+\epsilon)$, where $p_c = 1/(Z-1)$ and $\epsilon \ll 1$, we expect that the probability distribution $p_V(V)$ peaks around zero. Thus, we may expand the integrand in Eq. 54 around this value

$$\exp\left[-\frac{svV}{(v^n + V^n)^{1/n}} \right] = \exp[-sV] \left\{ 1 + \frac{s}{n} \frac{V^{n+1}}{v^n} + \cdots \right\} \quad (55)$$

and substitute to get the approximate equation

$$P_V(s) \simeq \left[1 - p + pP_v(s) + \frac{ps}{n} \int_0^\infty \frac{h(v)\, dv}{v^n} \times \int_0^\infty V^{n+1} \exp(-sV) p_V(V)\, dV \right]^{Z-1}. \quad (56)$$

We will seek the solution of Eq. 56 in the small ϵ limit as follows

$$P_V(s) = [R + \epsilon f(\epsilon^\lambda s)]^{z-1} \quad (57)$$

where the constant term R solves

$$R = 1 - p + pR^{Z-1} \quad (58)$$

and, near p_c, we have $R = 1 - [2/(Z-2)]\epsilon + \cdots$. Note that R denotes the probability of a branch being finite, and it is independent of n. The exponent $\lambda > 0$ will be determined by matching, as shown below.

Before we proceed, we make two remarks: First, we note that the unknown function f satisfies the two boundary conditions

$$f(0) = \frac{2}{Z-2} \quad (59)$$

obtained from Eq. 57 in the limit $s \to 0$, $\epsilon \neq 0$, in view of $P_V(0) = 1$, and

$$f(\infty) = 0 \quad (60)$$

in view of Eq. 58. Second, we note that the Laplace transform of the product $V^{n+1} p_V(V)$ can be related to that of P_V. This is shown in Appendix A, where we derive the relation

$$\int_0^\infty V^{n+1} p_V(V) e^{-sV}\, dV = \frac{(-1)^N}{\Gamma(1+N-\nu)} \int_0^\infty \frac{P_V^{(N)}(s+r)\, dr}{r^{\nu-N}} \quad (61)$$

where N is the integer part of $\nu \equiv n+2$, $\Gamma(z)$ is the Gamma function, and $P^{(N)}$ denotes the Nth derivative of P.

Consider, now, the substitution of Eqs. 61, 58, and 57 into Eq. 56 and take an expansion in powers of ϵ. In order to match at least $O(\epsilon^2)$, it can be shown after some algebra that the following two conditions must hold

$$\lambda = \frac{1}{n} \tag{62}$$

and

$$\frac{y(-1)^n}{n\Gamma(1+N-\nu)}\int_0^\infty \frac{h(v)\,dv}{v^n}\int_0^\infty \frac{f^{(N)}(y+\psi)\,d\psi}{\psi^{\nu-N}} + \left(f-\frac{2}{Z-2}\right)+\left(\frac{Z-2}{2}\right)\left(f-\frac{2}{Z-2}\right)^2 = 0 \tag{63}$$

where, we denoted $y = \epsilon^{1/n}s$. Equation 63 can be further rearranged using the rescaling

$$x = s\left[\frac{\epsilon}{\int_0^\infty (h/v^n)dv}\right]^{1/n} \quad \text{and} \quad \Phi = \left(\frac{Z-2}{2}\right)f \tag{64}$$

to lead to the nonlinear integrodifferential equation

$$\frac{(-1)^N x}{n\Gamma(1+N-\nu)}\int_0^\infty \frac{\Phi^{(N)}(x+\rho)\,d\rho}{\rho^{\nu-N}} = \Phi(1-\Phi) \tag{65}$$

subject to the boundary conditions

$$\Phi(0) = 1$$
$$\Phi(\infty) = 0. \tag{66}$$

In the case of integer n, Eq. 64 becomes an ODE

$$\frac{(-1)^{n+1}x}{n}\Phi^{(n+1)} = \Phi(1-\Phi), \tag{67}$$

a special case of which is the linear (Newtonian) limit $n = 1$, where Eq. 67 coincides with Stinchcombe's equation $x\Phi'' = \Phi(1-\Phi)$. It is also interesting to note that Eq. 67 has a singular limit at $n = 0$, which could be reached by some analytic continuation techniques. In this limit we obtain

$$\Phi = \lim_{n\to 0}\left(\frac{1}{1+Bx^n}\right) \tag{68}$$

where the constant B is to be determined (see below).

The solution of Eq. 65 is necessary for the determination of the conductivity of the system. To find the average conductance along $(Z-1)$ branches we shall use the expression (Stinchcombe, 1974) $\langle V\rangle = -(dP_v/ds)|_{s=0}$, which after some algebra gives

$$\langle V\rangle = -\frac{2}{(1-p_c)}p_c^{-\left(1+\frac{1}{n}\right)}\left[\int_0^\infty \frac{h(v)\,dv}{v^n}\right]^{-1/n} \times \frac{d\Phi}{dx}\bigg|_0 (p-p_c)^{1+(1/n)}. \tag{69}$$

The effective conductance of a bond, v_m, is related to $\langle V\rangle$ through Eq. 48 (where we make the identification $V^* = \langle V\rangle$). Thus,

$$v_m = -\frac{2}{(1-p_c)}\left[(1-p_c^n)p_c\int_0^\infty \frac{h(v)\,dv}{v^n}\right]^{-1/n} \times \frac{d\Phi}{dx}\bigg|_0 (p-p_c)^{1+(1/n)} \tag{70}$$

This expression provides the behavior of the effective conductance of a bond near the percolation threshold. We should point out that the scaling result $v_m \sim (p-p_c)^{1+(1/n)}$, was originally derived by Straley and Kenkel (1984). Here, we have also determined the precise prefactor, for the calculation of which Eq. 65 must be solved. It should be noted that in terms of the pore-size distribution, we can write

$$\int_0^\infty \frac{h(v)\,dv}{v^n} \sim \int_0^\infty \frac{\alpha(r)\,dr}{r^{3n+1}}.$$

Along with the other terms in Eq. 70, this can be used to infer the behavior of v_m as n vanishes.

The technique for the solution of Eq. 65 is shown in Appendix B. Fully forward finite differences were used to approximate the derivatives, and an asymptotic solution was also developed to start the integration. The two-point boundary-value problem was solved by a shooting method. Plotted in Figures 10 and 11 are the corresponding numerical results. Figure 10 shows a plot of Φ vs. x for different values of n. It is shown that Φ is almost independent of n at large n, but it becomes a very sensitive function of n at small values of the latter. As n decreases, the function Φ extends over considerably larger values of x. This is in agreement with the analytical limit (Eq. 68). The prefactor $\Phi'(0)$, which is needed in the evaluation of Eq. 70, is also rather insensitive to n for $n > 1$, but it becomes a sensitive function of n, decreasing in

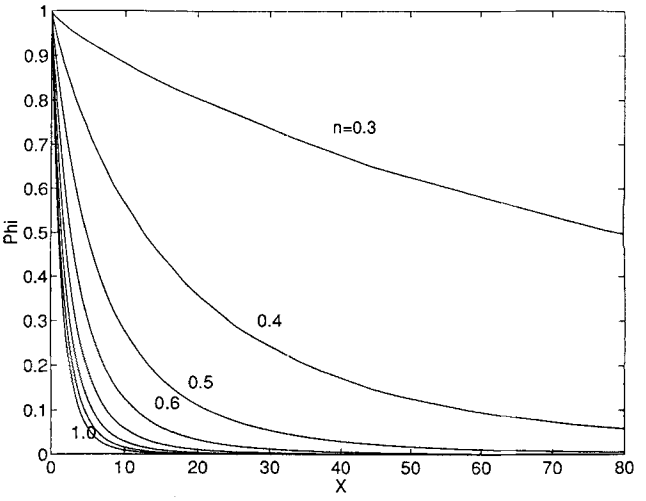

Figure 10. Solution of the integrodifferential equation (Eq. 65).

Φ plotted vs. x for different values of the power-law index.

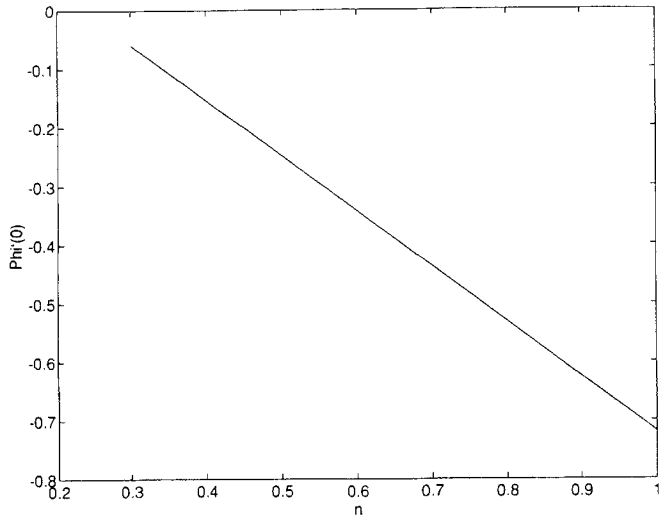

Figure 11. Solution of integrodifferential equation (Eq. 65).

Prefactor $\Phi'(0)$ plotted vs. the power-law index.

magnitude as n decreases below the value of 1 (Figure 11). The net effect is that the conductance decreases as n decreases. This plot can be used to deduce the exact behavior of the conductance for various values of n near percolation.

Conclusions

In this article, various aspects of the flow of power-law fluids in porous media were examined. First, it was shown using homogenization theory that a macroscopic power law between flow rate and pressure gradient applies at low Reynolds numbers, a regime that is reached at low velocities only if $n < 2$. The macroscopic power law has the same form as the power law for a single capillary. However, the power-law permeability may also depend on the pressure gradient orientation. The theory confirms the validity of a description of the flow of power-law fluids in porous media using pore networks. The latter method is not necessarily applicable, however, when more general rheologies are involved.

Subsequently, simulation in pore networks was used to explore various effects of the pore-size distribution on the macroscopic flow. Numerical simulations showed that approaches based on an effective medium or on the existence of a critical path, which carries most of the flow, are likely to arise when size distributions are narrow or wide, respectively. In particular, because of the sensitive dependence of the conductance on the pore size as the power-law index decreases, a critical path analysis is likely to be valid for general distributions, for sufficiently small n. Numerical solutions were used to test the two theories. An EMT was developed based on arguments valid for a Bethe lattice and found to agree reasonably with the numerical results over a large range of n, provided that the size distribution is sufficiently narrow. Alternatively, the CPA result of Sahimi and Yortsos (1990) was found to be in good agreement with the numerical results for sufficiently wide pore-size distributions. Because the latter is likely to be the case in many real porous media, the CPA result can be used to model such cases.

Finally, we used an analysis of flow in Bethe lattices to derive some closed-form expressions in two limits, one for an effective medium and another near percolation. The first result is useful for relatively large coordination numbers and was found to agree reasonably with the numerical results, as pointed out earlier. The behavior near percolation generalizes the results of Stinchcombe (1974) for the linear (Newtonian) case. More generally, these results are applicable to problems involving networks of power-law resistors. The general conclusion is that at low Re, power-law fluid flow in porous media leads to interesting new results as the power-law exponent n becomes small, the process being rather insensitive to n in the shear-thickening case. The special limit $n = 0$, which should have many common features with the flow of Bingham plastics, is discussed separately (Shah et al., 1995).

Acknowledgments

This research was partly supported by DOE Contract DE-FG22-90BC14600, the contribution of which is gratefully acknowledged. Adel Heiba contributed to the solution of Eq. 65 as described in Appendix B.

Notation

D_p = mean particle diameter
r = bond conductance
s = Laplace transform variable
t_n = power-law conductivity exponent
ϵ = asymptotic homogenization parameter
η = viscosity
ρ = density
$\tau_{1/2}$ = Ellis model parameter for shear stress

Literature Cited

Ambegaokar, V., B. I. Halperin, and J. S. Langer, "Hopping Conductivity in Disordered Systems," *Phys. Rev.*, **B4**, 2612 (1971).
Auriault, J. L., "Dynamic Behaviour of Porous Media Saturated by a Newtonian Fluid," *Int J. Eng. Sci.*, **18**, 775 (1980).
Auriault, J. L., "Dynamic Behaviour of Porous Media," *NATO ASI Ser.*, **202**, 471 (1991).
Barenblatt, G. I., V. M. Entov, and V. M. Ryzhik, *Theory of Fluid Flows through Natural Rocks*, Kluwer, Dordrecht, The Netherlands (1990).
Bender, C. M., and S. A. Orszag, *Advanced Mathematical Methods for Scientists and Engineers*, McGraw-Hill, New York (1978).
Bensoussan, A., J. L. Lions, and G. Papanicolaou, *Asymptotic Analysis for Periodic Structures*, North-Holland, Amsterdam (1978).
Bird, R. B., W. E. Stewart, and E. N. Lightfoot, *Transport Phenomena*, Wiley, New York (1960).
Blumenfeld, R., and A. Aharony, "Nonlinear Resistor Fractal Networks, Topological Distances, Singly Connected Bonds and Fluctuations," *J. Phys. A*, **18**, L443 (1985).
Blumenfeld, R., Y. Meir, B. Harris, and A. Aharony, "Infinite Set of Exponents for Describing Physics on Fractals," *J. Phys. A*, **19**, L791 (1986).
Bourgeat, A., and A. Mikelic, "Homogenization of Polymer Flow Through a Porous Medium," preprint (1992).
Cannella, W. J., C. Huh, and R. S. Seright, "Prediction of Xanthan Rheology in Porous Media," Tech. Conf. and Exhibition of the Soc. Plast. Eng., SPE 18089, Houston, Oct. 2–5 (1988).
Chauveteau, G., "Molecular Interpretation of Several Different Properties of Flow of Coiled Polymer Solutions Through Porous Media in Oil Recovery Conditions," Tech. Conf. and Exhibition of the Soc. Petr. Eng., SPE 10060, San Antonio, TX, Oct. 5–7 (1981).
Christopher, R. H., and S. Middleman, "Power-Law Flow Through Porous Media," *Ind. Eng. Chem. Fund.*, **4**, 422 (1965).

Deiber, J. A., and W. R. Schowalter, "Modeling the Flow of Viscoelastic Fluids Through Porous Media," *AIChE J.*, **27**, 921 (1981).
Duda, J. L., S. A. Hong, and E. E. Klaus, "Flow of Polymer Solutions in Porous Media: Inadequacy of the Capillary Model," *Ind. Eng. Chem. Fund.*, **22**, 299 (1983).
Durst, F., R. Haas, and W. Interthal, "The Nature of Flows Through Porous Media," *J. Non-Newtonian Fluid Mech.*, **22**, 169 (1987).
Fatt, I., "The Network Model of Porous Media," *Trans. AIME*, **207**, 160 (1956).
Heinrichs, G. I., and N. Kumar, "Simple Exact Treatment of Conductance in a Random Bethe Lattice," *J. Phys. C.*, **8**, L510 (1975).
Hirasaki, G. J., and G. A. Pope, "Analysis of Factors Influencing Mobility and Adsorption in the Flow of Polymer Solution Through Porous Media," *Soc. Pet. Eng. J.*, **14**, 337 (1974).
Huzarewicz, S., R. K. Gupta, and R. P. Chhabra, "Elastic Effects in Flow of Fluids Through Sinuous Tubes," *J. Rheol.*, **35**, 221 (1991).
James, D. F., and D. R. Mclaren, "The Laminar Flow of Dilute Polymer Solutions through Porous Media," *J. Fluid Mech.*, **70**, 733 (1975).
Jones, D. M., and K. Walters, "The Behavior of Polymer Solutions in Extension-Dominated Flows, With Applications to Enhanced Oil Recovery," *Rheol. Acta*, **28**, 482 (1989).
Katz, A. J., and A. H. Thompson, "Quantitative Prediction of Permeability in Porous Media," *Phys. Rev.*, **B34**, 8179 (1986).
Katz, A. J., and A. H. Thompson, "Prediction of Rock Electrical Conductivity from Mercury Injection Measurements," *J. Geophys. Res.*, **B92**, 599 (1987).
Koplik, J., "On the Effective Medium Theory of Random Linear Networks," *J. Phys. C*, **14**, 4821 (1981).
Koplik, J., "Creeping Flow in Two-Dimensional Network," *J. Fluid Mech.*, **119**, 219 (1982).
Larson, R. G., "Derivation of Generalized Darcy Equations for Creeping Flow in Porous Media," *Ind. Eng. Chem. Fund.*, **20**, 132 (1981).
Mei, C. C., and J. L. Auriault, "The Effect of Weak Inertia on Flow Through a Porous Media," *J. Fluid Mech.*, **222**, 647 (1991).
Pilitsis, S., A. Souvaliotis, A., and A. N. Beris, "Viscoelastic Flow in a Periodic Constricted Tube: The Combined Effect of Inertia, Shear Thinning and Elasticity," *J. Non-Newtonian Fluid Mech.*, **31**, 231 (1989).
Sadowski, T. J., "Non-Newtonian Flow Through Porous Media: I. Theoretical," *Trans. Soc. Rheol.*, **9**, 251 (1965).
Sadowski, T. J., and R. B. Bird, "Non-Newtonian Flow Through Porous Media: II. Experimental," *Trans. Soc. Rheol.*, **9**, 243 (1965).
Sahimi, M., "Nonlinear Transport Processes in Disordered Media," *AIChE J.*, **39**, 369 (1993).
Sahimi, M., and Y. C. Yortsos, "Flow of Non-Newtonian Fluids in Porous Media," *French Pet. Inst. Conf.*, Arles, France (1990).
Salman, M., "Factors Affecting Relative Permeabilities During Simultaneous Flow of Oil and Polymer Solutions Through Porous Media," PhD Thesis, Univ. of Southern California, Los Angeles (1989).
Savins, J. G., "Non-Newtonian Flow Through Porous Media," *Ind. Eng. Chem.*, **61**, 81 (1969).
Schurz, G. F., F. D. Martin, and R. Seright, "Polymer-Augmented Waterflooding and Control of Reservoir Heterogeneity," Symp. Petrol. Technol. into the Second Century, Socorro, New Mexico, Oct. 16–19 (1989).
Shah, C. B., and Y. C. Yortsos, "Aspects of Non-Newtonian Flow and Displacement in Porous Media," *DOE Topical Rep.* (1993a).
Shah, C. B., H. Kharabaf, and Y. C. Yortsos, "Flow and Displacement of Bingham Plastics in Porous Media," *Proc. Unitar Conf. on Heavy Oils and Tar Sands*, Houston (Feb. 16, 1995).
Sheffield, R. E., and A. B. Metzner, "Flows of Nonlinear Fluids Through Porous Media," *AIChE J.*, **22**, 736 (1976).
Simon, R., and F. J. Kelsey, "The Use of Capillary Tube Network in Reservoir Performance Studies: I. Equal-Viscosity Miscible Displacement," *Soc. Pet. Eng. J.*, 99 (1971).
Sorbie, K. S., P. J. Clifford, and E. R. W. Jones, "The Rheology of Pseudoplastic Fluids in Porous Media Using Network Modeling," *J. Colloid Interf. Sci.*, **130**, 508 (1989).
Sorbie, K. S., "Network Modeling of Xanthan Rheology in Porous Media in the Presence of Depleted Layer Effects," Tech. Conf. and Exhibition of Soc. Petr. Eng., SPE 19651, San Antonio, TX (Oct. 8–11, 1989).
Stinchcombe, R. B., "Conductivity and Spin-Wave Stiffness in Disordered Systems—An Exactly Soluble Model," *J. Phys.*, **C7**, 179 (1974).
Straley, J. P., and S. W. Kenkel, "Percolation Theory of Nonlinear Circuit Elements," *Phys. Rev. Lett.*, **49**, 767 (1982).
Straley, J. P., and S. W. Kenkel, "Percolation Theory for Nonlinear Conductors," *Phys. Rev.*, **B29**, 6299 (1984).
Teeuw, D., and F. Hesselink, "Power-Law Flow and Hydrodynamic Behavior of Biopolymer Solutions in Porous Media," Soc. Petr. Eng. Int. Symp. on Oilfield and Geothermal Chemistry, SPE 8982, Stanford, CA, May 28–30 (1980).
Willhite, G. P., and J. T. Uhl, "Correlation of the Flow of Flocon 4800 Biopolymer with Polymer Concentration and Rock Properties in Berea Sandstone," Amer. Chem. Soc. Meeting, Anaheim, CA, Sep. 8–11 (1986).
Wu, Y. S., K. Pruess, and P. A. Witherspoon, "Flow and Displacement of Bingham Non-Newtonian Fluids in Porous Media," *SPERE*, 369 (1992).
Wu, Y. S., K. Pruess, and P. A. Witherspoon, "Displacement of a Newtonian Fluid by a Non-Newtonian Fluid in a Porous Medium," *Trans. Porous Media*, **6**, 115 (1991).
Zaitoun, A., and G. Chauveteau, "Basic Rheological Behavior of Xanthan Polysaccharide Solutions in Porous Media: Effect of Pore Size and Polymer Concentration," *Proc. European Symp. on Enhanced Oil Recovery*, Bournemouth, England, Sep. 21–23 (1981).

Appendix A

In order to prove Eq. 61 we first note that its lefthand side (LHS) can be expressed as

$$\int_0^\infty V^{n+1}p(V)e^{-sV}\,dV = \int_0^\infty V^{n+1}e^{-sV}\left\{\frac{1}{2\pi i}\int_{\gamma-i\infty}^{\gamma+i\infty}P(s')e^{s'V}\,ds'\right\}dV \quad \text{(A1)}$$

where we dropped subscript V and defined the inverse Laplace transform in terms of contour integration as shown in Figure 12. Then, Eq. A1 can further be expressed as

$$\int_0^\infty V^{n+1}p(V)e^{-sV}\,dV = \frac{\Gamma(n+2)}{2\pi i}\int_{\gamma-i\infty}^{\gamma+i\infty}\frac{P(s')\,ds'}{(s-s')^{n+2}}. \quad \text{(A2)}$$

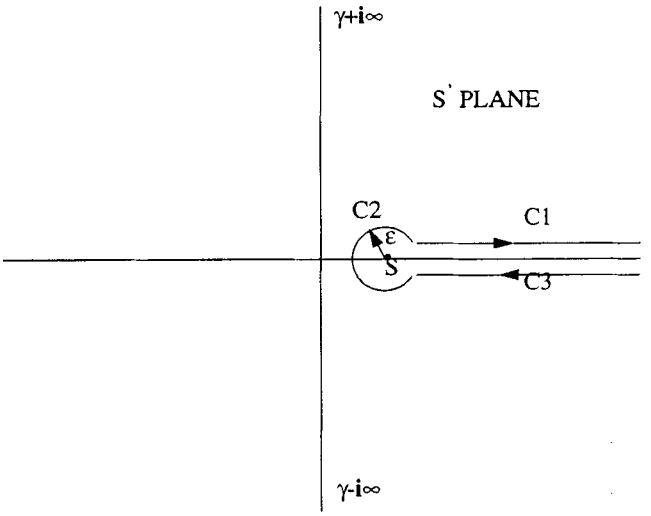

Figure 12. Contour integration.

To evaluate the righthand side (RHS) of Eq. A2 for arbitrary n, a branch cut is needed at $s' = s$ (Figure 12). After some calculations, the contribution of the integral from contours C_1 and C_3 is

$$\frac{\sin \nu\pi}{\pi} \int_{\epsilon}^{\infty} \frac{P(s+r)\, dr}{r^{\nu}} \tag{A3}$$

and that from contour C_2 is

$$\frac{\epsilon^{1-\nu}}{2\pi} \int_{-\pi}^{\pi} P(s - \epsilon e^{i\theta}) e^{i\theta(1-\nu)}\, d\theta \tag{A4}$$

where $\nu \equiv n+2$.

If ν is an integer, only the latter contributes. A Taylor series expansion of P

$$\int_{-\pi}^{\pi} P(s - \epsilon e^{i\theta}) e^{i\theta(1-\nu)}\, d\theta = \int_{-n}^{n} \left[P(s) - \epsilon e^{i\theta} P'(s) + \cdots + \frac{(-1)^k}{k!} \epsilon^k e^{ik\theta} P^{(k)}(s) + \cdots \right] e^{i\theta(1-\nu)}\, d\theta \tag{A5}$$

shows that the only contributing term is the kth term, where $k = \nu - 1$. Then, we can readily show that

$$\int_0^{\infty} V^{n+1} p(V) e^{-sV}\, dV = (-1)^{n+1} P^{(n+1)}(s) \tag{A6}$$

in this case.

If ν is not an integer, we let m denote the next largest integer, $m = [\nu] + 1$. Note that $m \geq 3$. In the limit $\epsilon \to 0$, terms in A3 with $k > \nu' - 1$ do not contribute and the series terminates at $k^* = m - 2$. Therefore, A2 becomes

$$\int_0^{\infty} V^{n+1} p(V) e^{-sV}\, dV = \frac{\Gamma(\nu) \sin \nu\pi}{\pi} \times \int_0^{\infty} \left(\frac{P(s+r)}{r^{\nu}} - \sum_0^{m-2} \frac{r^{k-\nu} P^{(k)}(s)}{k!} \right) dr. \tag{A7}$$

Successive integrations by parts yields

$$\int_0^{\infty} \left(\frac{P(s+r)}{r^{\nu}} - \sum_0^{m-2} \frac{r^{k-\nu} P^{(k)}(s)}{k!} \right) dr = \frac{1}{(\nu-1)\cdots(\nu-N)} \int_0^{\infty} \frac{P^{(N)}(s+r)\, dr}{r^{\nu-N}} \tag{A8}$$

where $N = [\nu]$. Substitution of Eq. A8 into Eq. A7 gives Eq. 61 in the main text.

Appendix B

To solve Eq. 65, we first develop an asymptotic solution at large x, where it can be approximated by the linear equation

$$\frac{(-1)^N x}{n\Gamma(1+N-\nu)} \int_0^{\infty} \frac{\Phi^{(N)}(x+\rho)\, d\rho}{\rho^{\nu-N}} = \Phi. \tag{B1}$$

An asymptotic analysis of Eq. B1 requires the use of the Liouville substitution

$$\Phi = A \exp[S(x)] \tag{B2}$$

and the approximation of derivatives by the leading-order expression (see Bender and Orszag, 1978)

$$\Phi^{(N)}(x) \sim (S')^N \exp[S(x)] + \cdots. \tag{B3}$$

Substitution of Eqs. B3 and B2 into Eq. B1 and use of standard approximation techniques for the asymptotic evaluation of the various integrals, including Watson's lemma (Bender and Orszag, 1978), gives

$$S(x) = -ax^b a = (n+1) n^{-n/(n+1)}$$
$$b = \frac{n}{n+1}. \tag{B4}$$

For any n, the asymptotic solution provides Φ and its derivatives at large x to within a constant A. This information is used as an initial condition for the integration of Eq. 64 in the direction of decreasing x, starting from a suitably large x. Derivatives in Eq. 64 are evaluated by a completely forward formulation, so that at each step only one unknown exists. The solution is then compared to $\Phi(0) = 1$ and iteration in A is made until matching is obtained. Although the solution of the problem is straightforward for $n > 1$, it becomes considerably stiff for smaller values of n. In the latter case, we made use of the transformation suggested by the asymptotic result (Eqs. B2 and B4), and introduced $z = ax^b$ in the full equation.

Manuscript received Dec. 28, 1993, and revision received May 26, 1994.